Annals of Biomedical Engineering, Vol. 36, No. 1, January 2008 *(© 2007)* pp. 41–56
DOI: 10.1007/s10439-007-9405-8

Electrophysiological Modeling of Fibroblasts and their Interaction with Myocytes

FRANK B. SACHSE, ALONSO P. MORENO, and J. A. ABILDSKOV

Nora Eccles Harrison Cardiovascular Research and Training Institute, University of Utah, 95 S 2000 E, Salt Lake City, UT 84112, USA

(Received 7 December 2006; accepted 2 November 2007; published online 13 November 2007)

Abstract—Experimental studies have shown that cardiac fibroblasts are electrically inexcitable, but can contribute to electrophysiology of myocardium in various manners. The aim of this computational study was to give insights in the electrophysiological role of fibroblasts and their interaction with myocytes. We developed a mathematical model of fibroblasts based on data from whole-cell patch clamp and polymerase chain reaction (PCR) studies. The fibroblast model was applied together with models of ventricular myocytes to assess effects of heterogeneous intercellular electrical coupling. We investigated the modulation of action potentials of a single myocyte varying the number of coupled fibroblasts and intercellular resistance. Coupling to fibroblasts had only a minor impact on the myocyte's resting and peak transmembrane voltage, but led to significant changes of action potential duration and upstroke velocity. We examined the impact of fibroblasts on conduction in one-dimensional strands of myocytes. Coupled fibroblasts reduced conduction and upstroke velocity. We studied electrical bridging between ventricular myocytes via fibroblast insets for various coupling resistors. The simulations showed significant conduction delays up to 20.3 ms. In summary, the simulations support strongly the hypothesis that coupling of fibroblasts to myocytes modulates electrophysiology of cardiac cells and tissues.

Keywords—Computational modeling, Fibroblast, Cardiac electrophysiology, Electrical bridging.

INTRODUCTION

Fibroblasts are by number the predominant cardiac cell type and organized in a three-dimensional network in the myocardium.[16] Fibroblasts are the primary producer of myocardial extracellular matrix proteins.[12] Additionally, they seem to play a role in cardiac electrophysiology. Several cardiac diseases are associated with activation of fibroblasts and transitions of their phenotype.[2] Myocardial infarction and injury activate fibroblasts as major player of the healing response, but chronic activation can lead to fibrosis, hypertrophy, and heart failure.[31] In the aged and hypertrophic heart, fibroblasts produce collagenous septa, which can act as barriers for electrical conduction.

Cardiac fibroblasts are electrically inexcitable, but can contribute to the electrophysiology of myocytes in various manners. Electrical coupling via fibroblasts was hypothesized to underlie synchronization of contraction among individual myocytes, which was reported in early studies of cells cultures from mouse and rat embryos.[17,20] Electrical coupling of fibroblasts and myocytes was demonstrated at cellular and tissue level as well as in cell cultures.[7,14,27,37] Coupling of fibroblasts to myocytes was reported via Cx43 gap junctions in sheep ventricular and via Cx45 in rabbit sinoatrial node cells.[5,26] Resistances between myocytes and fibroblasts in the range of 125 and 3225 MΩ have been measured in cell culture of neonatal rat cardiac cells.[37] Fibroblast–myocyte coupling via both types of gap junctions has been demonstrated in sheep ventricular scars.[4] Additionally, fibroblast–fibroblast coupling via Cx40 gap junctions and a resistance in the range of 166 and 5714 MΩ have been reported in culture of neonatal rat cells.[6,37] Resistances in myocyte–fibroblast and fibroblast–fibroblast pairs are significantly smaller than in myocyte pairs. For instance, a mean resistance of 5.7 and 5.9 MΩ has been measured in pairs of rabbit ventricular and atrial myocytes, respectively.

Several studies suggested electrical bridging of myocytes by fibroblasts.[7,14,37] Synchronous contraction in myocyte–fibroblast–myocyte triplets associated with a summary resistance between 333 and 6666 MΩ have been found for culture of neonatal rat cardiac cells.[37] In a similar preparation, conduction over distances up to 300 μm along fibroblast inserts with delays of up to 68 ms and apparent conduction velocities of 4.6 ± 1.8 mm/s were reported.[14]

Address correspondence to Frank B. Sachse, Nora Eccles Harrison Cardiovascular Research and Training Institute, University of Utah, 95 S 2000 E, Salt Lake City, UT 84112, USA. Electronic mail: fs@cvrti.utah.edu

The role of fibroblasts as electrical bridges between myocytes still remains to be clarified.[38] A beneficial role was proposed by reason that fibroblasts can increase electrical coupling of myocytes, which are separated by collagenous septa and scars. Contrarily, electrical bridges were found to be arrhythmogenic in various studies of Purkinje fibers as well as of atrial and ventricular tissue.[1,9–11,47,48] These studies were carried out with preparations with segmental depressed excitability and showed in particular slowed conduction and reflected reentry.

The aim of this study was to give insights in the electrophysiological role of fibroblasts and their interaction with myocytes. The study was carried out with mathematical models and computational simulations of cellular and multi-cellular electrophysiology. We developed a novel mathematical model of cardiac fibroblasts on basis of data from recent whole-cell patch clamp and polymerase chain reaction (PCR) studies. The fibroblast model was applied together with models of ventricular myocytes to assess electrophysiological effects of heterogeneous electrical coupling of cells. We investigated the modulation of the action potentials of single myocytes by connected fibroblasts and electrical bridging between ventricular myocytes via fibroblasts. We developed protocols to quantify conduction delays and attempted to determine conditions for reflected reentry.

METHODS

Fibroblast Model Development

Our model describes the transmembrane voltage and currents of fibroblasts on basis of electrophysiological and PCR studies of isolated ventricular cells from adult male rats.[8,43] These studies indicated that two K^+ currents, an inwardly rectifying current I_{Kir} and a time- and voltage dependent outward current I_{Shkr}, are major determinants of the fibroblast's voltage–current relationship. In addition, our model describes an unspecific background current I_b responsible for maintaining the resting transmembrane voltage and includes a stimulus current I_{stim}. The membrane of a fibroblast is considered as introduced by Hodgkin–Huxley as an isopotential compartment with the membrane capacity C_m and transmembrane voltage V_m, which is a function of transmembrane currents:

$$\frac{\partial}{\partial t} V_m = -\frac{1}{C_m}(I_{Kir} + I_{Shkr} + I_b + I_{stim})$$

Electrophysiological studies have shown that the inwardly rectifying current I_{Kir} is nearly instantaneous, modulated by the external K^+ concentration, and can be blocked by $BaCl_2$.[8] PCR measurements have indicated that channels consisting of Kir subunits are the major carrier of this current. We described the current I_{Kir} by re-parameterizing a model for I_{K1} in cardiomyocytes[21]:

$$I_{Kir} = G_{Kir} O_{Kir} \sqrt{[K^+]_o}(V_m - E_K)$$

with the conductance G_{Kir} and the reversal voltage E_K. The channel open probability O_{Kir} was defined as:

$$O_{Kir} = \frac{1}{a_{Kir} + \exp(b_{Kir}(V_m - E_K)F/RT)}$$

with the constants a_{Kir} and b_{Kir}. The reversal voltage E_K is given by the Nernst equation for K^+:

$$E_K = \frac{RT}{F} \ln \frac{[K^+]_o}{[K^+]_i}$$

with constants as described in Tables 1 and 2. The conductance G_{Kir} was set according to results of whole cell voltage clamp experiments[8] (Table 1).

The outward current I_{Shkr} of fibroblasts was found to be time- and voltage dependent. PCR measurements suggested that this current passes through channels consisting of subunits in the Kv 1.*x* family (Shaker), which shows delayed rectifier and relatively slow inactivation properties. We reconstructed this current based on the Goldman–Hodgkin–Katz current equations[19] and a Markovian model of delayed rectifier K^+

TABLE 1. Constants of fibroblast model.

Parameter	Symbol	Value
Temperature (K)	T	295
Membrane capacity (pF)	C_m	4.50
Intracellular K^+ concentration (mM)	$[K^+]_i$	140
I_{kir} parameter	a_{Kir}	0.94
I_{kir} parameter	b_{Kir}	1.27
Conductance for I_{kir} (nS)	G_{Kir}	1.02
I_{shkr} parameter (s^{-1})	k_{v0}	30
I_{shkr} parameter	z_v	1.28
I_{shkr} parameter (s^{-1})	k_{-v0}	2
I_{shkr} parameter	z_{-v}	–1.53
I_{shkr} parameter (s^{-1})	k_o	77
I_{shkr} parameter (s^{-1})	k_{-o}	18
Membrane permeability to I_{shkr} (m^3/s)	P_{Shkr}	$5.40 \cdot 10^{-15}$
Maximum conductance of background current I_b (pS)	G_b	6.9
Reversal voltage of background current I_b (mV)	E_b	0.00

TABLE 2. Physical constants.

Name	Symbol	Value
Faraday's constant (C mol^{-1})	F	$9.65 \cdot 10^4$
Gas constant (J K^{-1} mol^{-1})	R	8.31

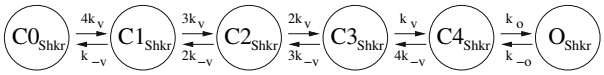

FIGURE 1. Schematic of Markovian model for the time- and voltage dependent outward current I_{Shkr} (modified from[25]). The model describes probabilities for six different states of an ion channel, i.e., five closed states, $C0_{Shkr} - C4_{Shkr}$, and an open state O_{Shkr}.

currents and its parameterization for shaker channels in neurons[25,49] (Fig. 1):

$$I_{\mathrm{Shkr}} = P_{\mathrm{Shkr}} O_{\mathrm{Shkr}} \frac{V_{\mathrm{m}} F^2}{RT} \frac{[\mathrm{K}^+]_i - [\mathrm{K}^+]_{\mathrm{o}} \exp(-V_{\mathrm{m}} F/RT)}{1 - \exp(-V_{\mathrm{m}} F/RT)}$$

with the permeability P_{Shkr} and the probability of the open state O_{Shkr}. The Markovian model describes five closed states, $C0_{\mathrm{Shkr}} \ldots C4_{\mathrm{Shkr}}$, and one open state O_{Shkr}:

$$\frac{\partial}{\partial t} C0_{\mathrm{Shkr}} = -4k_{\mathrm{v}} C0_{\mathrm{Shkr}} + k_{-\mathrm{v}} C1_{\mathrm{Shkr}}$$
$$\frac{\partial}{\partial t} C1_{\mathrm{Shkr}} = 4k_{\mathrm{v}} C0_{\mathrm{Shkr}} - (3k_{\mathrm{v}} + k_{-\mathrm{v}}) C1_{\mathrm{Shkr}} + 2k_{-\mathrm{v}} C2_{\mathrm{Shkr}}$$
$$\frac{\partial}{\partial t} C2_{\mathrm{Shkr}} = 3k_{\mathrm{v}} C1_{\mathrm{Shkr}} - (2k_{\mathrm{v}} + 2k_{-\mathrm{v}}) C2_{\mathrm{Shkr}} + 3k_{-\mathrm{v}} C3_{\mathrm{Shkr}}$$
$$\frac{\partial}{\partial t} C3_{\mathrm{Shkr}} = 2k_{\mathrm{v}} C2_{\mathrm{Shkr}} - (k_{\mathrm{v}} + 3k_{-\mathrm{v}}) C3_{\mathrm{Shkr}} + 4k_{-\mathrm{v}} C4_{\mathrm{Shkr}}$$
$$\frac{\partial}{\partial t} C4_{\mathrm{Shkr}} = k_{\mathrm{v}} C3_{\mathrm{Shkr}} - (k_{\mathrm{o}} + 4k_{-\mathrm{v}}) C4_{\mathrm{Shkr}} + k_{-\mathrm{o}} O_{\mathrm{Shkr}}$$
$$\frac{\partial}{\partial t} O_{\mathrm{Shkr}} = k_{\mathrm{o}} C4_{\mathrm{Shkr}} - k_{-\mathrm{o}} O_{\mathrm{Shkr}}$$

The rate coefficients k_{v} and $k_{-\mathrm{v}}$ are exponential functions of the transmembrane voltage V_{m}:

$$k_{\mathrm{v}} = k_{\mathrm{v0}} \exp(V_{\mathrm{m}} z_{\mathrm{v}} F/RT)$$
$$k_{-\mathrm{v}} = k_{-\mathrm{v0}} \exp(V_{\mathrm{m}} z_{-\mathrm{v}} F/RT)$$

with the parameters k_{v0} and $k_{-\mathrm{v0}}$ describing associated rate coefficients at 0 mV, and the apparent amount of charge moved between states z_{v} and $z_{-\mathrm{v}}$. The rate coefficients k_{o} and $k_{-\mathrm{o}}$ are constants. The parameters k_{v0}, $k_{-\mathrm{v0}}$, k_{o0}, and $k_{-\mathrm{o0}}$ were adjusted to reconstruct experimental studies of the activation kinetics at various $[\mathrm{K}^+]_{\mathrm{o}}$ (Fig. 2). Initial values of the states $C0_{\mathrm{Shkr}} - C4_{\mathrm{Shkr}}$, and O_{Shkr} for resting voltage are given in Table 3.

A description of an unspecific background current I_{b} was added to the fibroblast model. Background currents are usually observed in whole cell patch-clamp experiments, e.g., with rat kidney fibroblasts.[18] The background current I_{b} was described as in previous ohmic models of kidney and cardiac fibroblasts[28,45]:

$$I_{\mathrm{b}} = G_{\mathrm{b}}(V_{\mathrm{m}} - E_{\mathrm{b}})$$

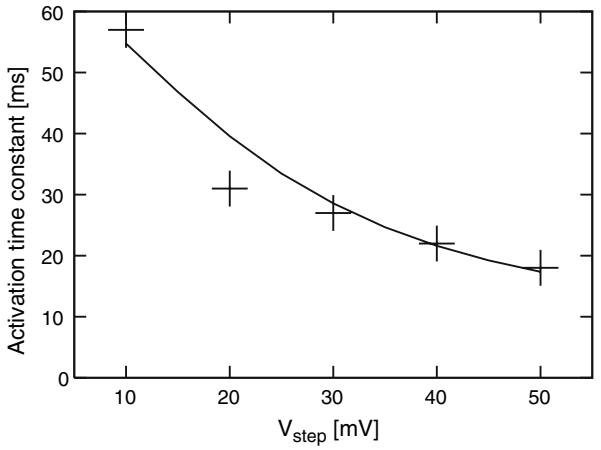

FIGURE 2. Activation kinetics of time- and voltage dependent outward current I_{Shkr} for $[K^+]_o$ = 5 mM. A voltage clamp protocol was applied to characterize activation time constants. Fibroblasts were initially clamped at −90 mV. Voltage steps V_{step} caused activation of the current I_{Shkr}, which is characterized by activation time constants. Crosses (+) indicate measured data.[43] Simulated data are represented with the closed line.

TABLE 3. Initial values of fibroblast model for $[K^+]_o$ = 5 mM.

Parameter	Symbol	Value
Transmembrane voltage (mV)	V_{m}	−58.00
0th Closed I_{shkr} state	$C0_{\mathrm{Shkr}}$	$9.11 \cdot 10^{-1}$
1st Closed I_{shkr} state	$C1_{\mathrm{Shkr}}$	$8.57 \cdot 10^{-2}$
2nd Closed I_{shkr} state	$C2_{\mathrm{Shkr}}$	$3.02 \cdot 10^{-3}$
3rd Closed I_{shkr} state	$C3_{\mathrm{Shkr}}$	$4.74 \cdot 10^{-5}$
4th Closed I_{shkr} state	$C4_{\mathrm{Shkr}}$	$2.79 \cdot 10^{-7}$
Open I_{shkr} state	O_{Shkr}	0

The reversal potential E_{b} was set to 0 mV[18] and the background conductance G_{b} was adjusted to fix the resting voltage of an isolated fibroblast to −58 mV for $[\mathrm{K}^+]_{\mathrm{o}}$ = 5 mM[43] (Fig. 3).

The system of ordinary differential equations underlying the fibroblast model was solved with the forward Euler method using a time step of 1 μs.[36] All calculations were performed in double precision floating point arithmetic.

Fibroblast–Myocyte Models

Fibroblast–myocyte interactions were studied by computational experiments, in which electrophysiological models of rat left ventricular subepicardial myocytes[34] and the upper fibroblast model were electrically connected by resistors. The resistors describe the intracellular space and the intercellular coupling via gap junctions. We configured four experimental arrangements (Fig. 4):

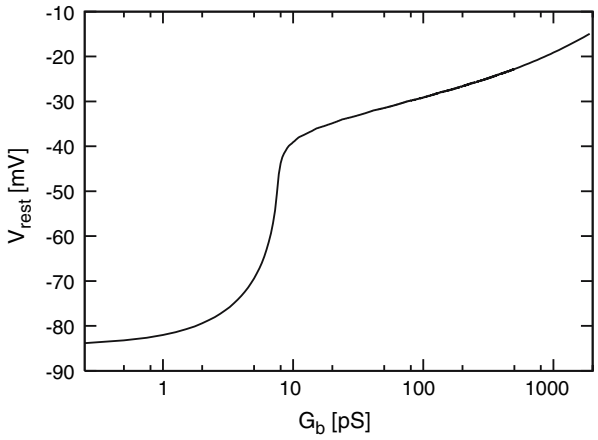

FIGURE 3. Effect of conductance G_b of the unspecific background current I_b on resting voltage V_{rest} of an isolated fibroblast.

- a single myocyte connected to a number of fibroblasts (M–F$_n$),
- a chain of myocytes coupled to an array of fibroblasts (M$_m$–F$_{nxm}$),
- two chains of myocytes connected by a chain of fibroblasts (M$_m$–F$_n$–M$_m$), and
- two chains of myocytes with ohmic coupling (M$_m$–M$_m$).

We varied in the computational experiments with these arrangements, the number of fibroblasts n, the resistor between myocytes and fibroblasts R_{mf}, and if applicable in-between fibroblasts R_{ff}, myocytes R_{mm}, and chains R_{cc}.

The arrangement M–F$_n$ (Fig. 4a) served to characterize and quantify the impact of various coupling myocyte–fibroblast resistors R_{mf} and the number of coupled fibroblasts n on the resting and action potential of a myocyte. Coupling resistances R_{mf} of 100 MΩ,1 GΩ, and 10 GΩ were chosen as an estimate of high, average and marginal coupling, respectively. Further simulations with a coupling resistance R_{mf} of 10 MΩ were performed to explore a case of extremely high coupling.

The arrangement M$_m$–F$_{nxm}$ (Fig. 4b) allowed us to study the effect of fibroblasts on conduction velocity in myocardium. Myocyte–myocyte coupling was reconstructed by a resistor R_{mm} of 6 MΩ. The myocyte–fibroblast resistor R_{mf} was set to 10 MΩ,100 MΩ,1 GΩ, and 10 GΩ. The measurement of conduction velocity was based on the detection of activation times for the 8th and 24th myocyte and assuming a myocyte length of 120 μm. The time of maximal upstroke velocity of the transmembrane voltage determined activation time.

The arrangement M$_m$–F$_n$–M$_m$ (Fig. 4c) was used to provide insights in the role of fibroblasts for electrical bridging between myocytes. Myocyte–myocyte resistors R_{mm} and myocyte–fibroblast resistors R_{mf} were systematically varied in the range of 1−100 MΩ. The fibroblast—fibroblast resistor R_{ff} was set identical to the myocyte–fibroblast resistor R_{mf}. This decision reduced the dimensionality of parameter variation from 3 to 2. Maximal conduction delays for each R_{mm} were detected with a bisection method for searching maxima in monotonic increasing function of.[36] The stopping criterion for the search was that the difference between two successively determined resistances R_{mf} was smaller than 1 Ω.

Similar studies were carried out with arrangement M$_m$–M$_m$ (Fig. 4d). Here, the myocyte–myocyte resistors R_{mm} and chain–chain resistor R_{cc} were varied searching for maximal conduction delays.

Conduction in cell strands was modeled by spatial finite difference discretization of the cable equation[3]:

$$\frac{a}{2}\frac{\partial}{\partial x}\left(\frac{1}{\rho(x)}\frac{\partial V_m(x,t)}{\partial x}\right) = I_{ion} + C_m\frac{\partial V_m(x,t)}{\partial t}$$

with the fiber radius a (8 μm), specific membrane capacity C_m, resistivity ρ, summary membrane current I_{ion} and transmembrane voltage V_m. The resistivity was calculated from the upper resistors R_{mm}, R_{mf}, R_{ff}, and R_{cc}. Neumann boundary conditions were assigned at the ends of strands. The spatial discretization was set similar to reported mean cell lengths: in regions with myocytes to 120 μm and with fibroblasts to 8 μm.

The ordinary differential equations underlying the arrangements were solved using the Euler method with a time step of 1 μs.[36] Intercellular currents were updated every 1 μs. In all simulations a stimulus frequency of 0.5 Hz was chosen. A stimulus current of 5 nA was applied to myocyte 0 until a threshold voltage was reached. The threshold voltage was −50 mV and −30 mV for the M–F$_n$ and other arrangements, respectively. The resulting stimulus duration was kept shorter than the duration of 5 ms used by Pandit *et al.*[34] to avoid significant overlap of sodium and stimulus current. Simulation results were analyzed after the 10th stimulation.

RESULTS

Fibroblast Model

An electrophysiological model of cardiac fibroblasts was developed based on measurements of isolated rat ventricular fibroblasts.[8,43] Measured and simulated voltage–current relationships for $[K^+]_o$ = 5, 10, 50, and 100 mM are shown in Fig. 5d and 5e, respectively. The voltage–current relationships describe steady-state currents for a voltage clamping protocol, where volt-

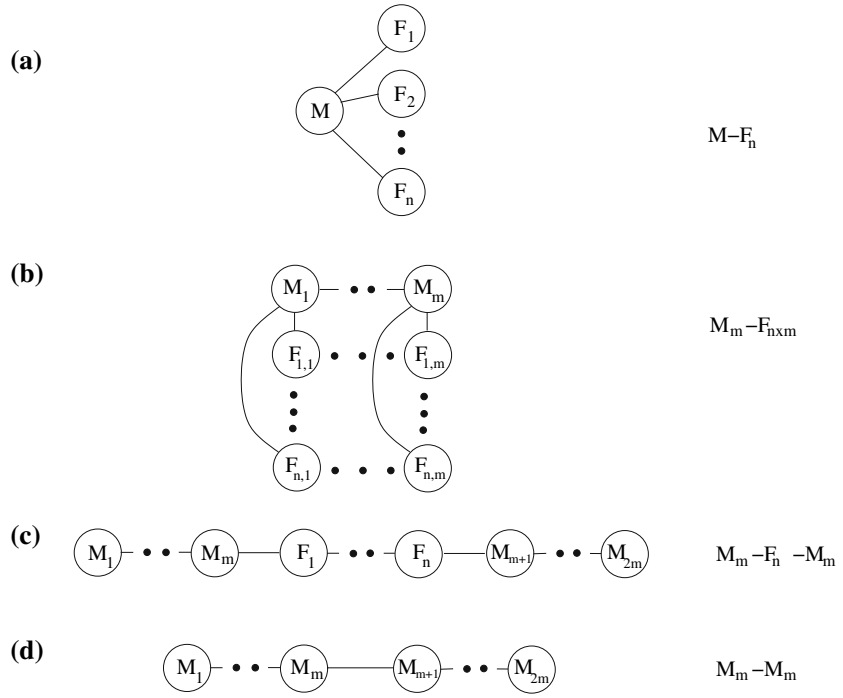

FIGURE 4. Arrangements of myocytes and fibroblasts for computational studies.

ages steps varied between −110 and 50 mV (Fig. 5a). Exemplary measured and simulated currents are demonstrated in Fig. 5b and 5c, respectively, for these voltage steps and $[K^+]_o = 10$ mM.

Major currents of our model were constituted by the inwardly rectifying current I_{Kir} (Fig. 6a) and the time- and voltage dependent outward current I_{Shkr} (Fig. 6b), which dominated the voltage–current relationships in the lower and upper range of the transmembrane voltage V_m, respectively. For physiological $[K^+]_o$ (≈ 5 mM) the lower and upper voltage range was defined as $V_m < -90$ mV and $V_m > -40$ mV, respectively. The unspecific background current I_b contributed little (relative to I_{Kir} and I_{Shkr}) to the summary voltage–current relationship (Fig. 6c) in the upper and lower voltage ranges. The current I_b was significant only outside of these ranges and caused deviations of the resting voltage of fibroblasts (–59 mV in case of physiological $[K^+]_o$) from the K^+ reversal potential.

Single Myocyte Coupled to Fibroblasts

Simulated transmembrane voltages of myocytes and fibroblasts are demonstrated in Fig. 7a and 7b for the case of high intercellular coupling with a resistance R_{mf} of 100 MΩ. The transmembrane voltage of the fibroblasts followed closely the transmembrane voltage of the myocyte. The action potential duration at 50% repolarization (APD_{50}) progressively increased from 14.9 ms to 22.6 ms as the number of fibroblasts n increased (Fig. 7f). Similarly, the action potential duration to 90% repolarization (APD_{90}) increased from 38.9 ms to 61.3 ms as the number of fibroblasts n increased.

Electrical coupling led to intercellular currents I_{inter}, which flowed during stimulus and action potential upstroke from the myocyte to the fibroblasts (Fig. 7c, d). The summary current I_{inter} from and to the myocyte increased as the number of fibroblasts n increased. Intercellular currents from myocyte to fibroblasts increased their transmembrane voltage by charging the membrane capacitor. Subsequently, the membrane capacitor of the fibroblasts was discharged and the current flowed reversed. This current was prominent only at period of the action potential notch and repolarization.

We characterized availability of sodium channels as product of fast and slow inactivation gating variables of I_{Na} (Fig. 7e). Increasing fibroblast number prolonged inactivation. The delay after stimulus to reappearance of 1% availability was 47.7, 50.3, 60.8, and 74.1 ms for 0, 1, 5, and 10 coupled fibroblasts.

In order to explore the role of intercellular coupling in modulation of action potentials, further simulations were performed with an intercellular resistances R_{mf} of 10 MΩ,1 GΩ, and 10 GΩ (Fig. 8). Similar transmembrane voltages and APDs as for a coupling resistance $R_{mf} = 100$ MΩ were found for a simulation with a

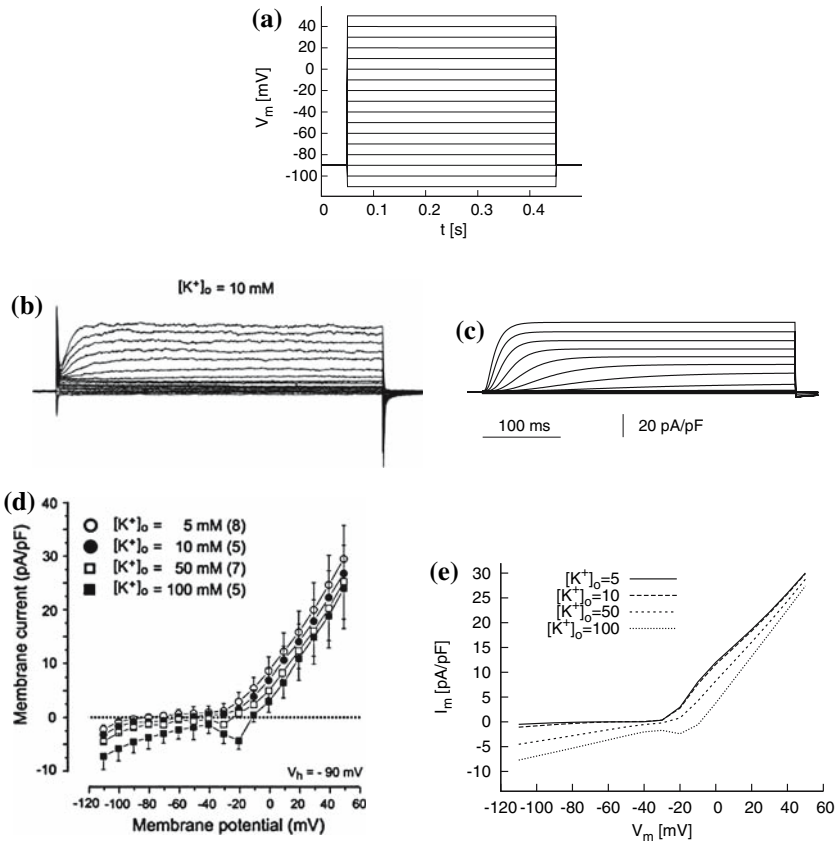

FIGURE 5. Reconstruction of voltage–current relationships of fibroblasts. (a) Voltage steps between −110 and 50 mV were applied for a duration of 400 ms from a holding potential of −90 mV. (b) Measured transmembrane currents I_m exhibit slow activation and no apparent inactivation. Data for $[K^+]_o$ = 10 mM are shown. (c) Simulated transmembrane currents I_m reconstruct the measured data. Scales for time and current in (b) and (c) are identical. Stationary currents were extracted for the different voltage steps and $[K^+]_o$ giving (d) measured and (e) simulated voltage–current relationships. (Figures with measured data are from[43]).

resistance $R_{mf} = 10\,M\Omega$ (Fig. 8a–c). In case of resistances $R_{mf} \geq 1\,G\Omega$ the transmembrane voltage of fibroblasts did not resemble the voltage of the myocyte (Fig. 8e, h). Marginal electrical coupling, $R_{mf} = 10\,G\Omega$, led to negative *n*-APD relationships (Fig. 8i). The APD_{50} and APD_{90} decreased from 14.9 to 13.6 ms and from 39.0 to 37.1 ms, respectively, as the number of fibroblasts *n* increased.

Resting transmembrane voltages and maximal upstroke velocities are presented in Fig. 9 dependent on the number of coupled fibroblasts. The resting voltage of a myocyte without coupled fibroblasts was −81.1 mV (Fig. 9a). The membrane voltage was increasingly depolarized with increasing number of coupled fibroblasts, though the changes were marginal. The most depolarized membrane voltage corresponded to a resistor $R_{mf} = 10\,M\Omega$ and coupling to 10 fibroblasts, which caused depolarization to −80.6 mV. The maximal upstroke velocity dV/dt_{max} of an uncoupled myocyte was 160 V/s (Fig. 9b). With 10 coupled fibroblasts, the velocity decreased to 114, 130, 150, and 157 V/s in case of $R_{mf} = 10\,M\Omega, 100\,M\Omega, 1\,G\Omega$ and $10\,G\Omega$, respectively.

For the purpose of characterizing intercellular coupling and feedback mechanisms, charge movement into a myocyte via sodium channels Q_{INa} and gap junctions Q_{IInter} was calculated by integrating the current flow from the time of upstroke to 95% repolarization of the fibroblast (Fig. 10). Increasing R_{mf} reduced the magnitude of Q_{INa}. In the extreme case of marginal coupled fibroblasts, Q_{INa} was independent of the number *n*. Otherwise, increasing *n* linearly increased the magnitude of Q_{INa}. The relationship between *n* and Q_{IInter} was linear for each R_{mf}. An increase of R_{mf} reduced Q_{IInter} for each *n*. Marginally coupled fibroblasts provided an electrical source, otherwise fibroblasts acted as a sink for the myocyte.

Conduction Velocity Modulated by Fibroblasts

Electrical conduction was simulated in a strand of 32 myocytes each coupled to a number of fibroblasts.

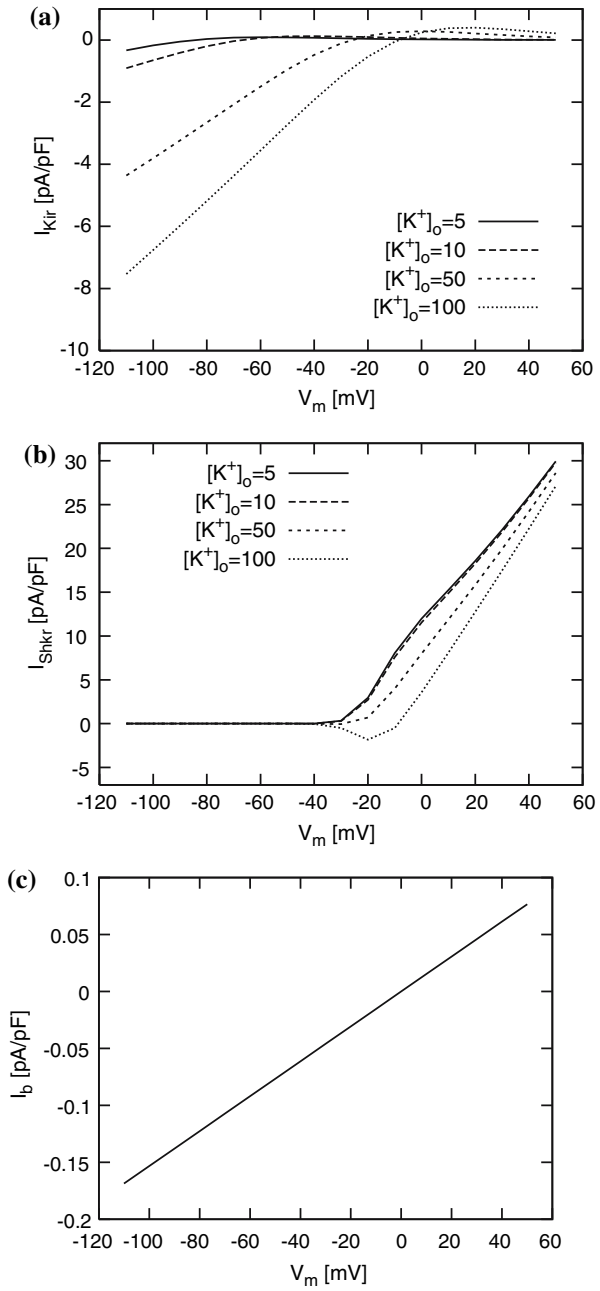

FIGURE 6. Decomposition of simulated voltage–current relationships. The transmembrane current I_m is mainly composed of two K^+ currents: (a) the inwardly rectifying current I_{Kir} and (b) the time- and voltage dependent outward current I_{Shkr}. (c) The contribution of the unspecific background current I_b is relatively small.

Conduction velocity v and maximal upstroke velocity dV/dt_{max} were determined (Fig. 11). For a myocyte–myocyte resistance R_{mm} of 6 MΩ, increasing numbers of coupled fibroblasts decreased conduction velocity v and upstroke velocity dV/dt_{max} of myocytes.

Conduction velocity v in the strand without coupled fibroblasts was 0.211 m/s (Fig. 11a). In case of 10 coupled fibroblasts, conduction velocity v was reduced to 0.150, 0.163, 0.198, and 0.208 m/s for myocyte–fibroblast resistances R_{mf} of 10 MΩ,100 MΩ,1 GΩ and 10 GΩ, respectively.

Upstroke velocity dV/dt_{max} in a central myocyte without fibroblasts coupled to the strand was 128.4 V/s (Fig. 11b). Coupling with 10 fibroblasts caused a reduction of the upstroke velocity dV/dt_{max} to 91.8, 99.7, 119.2, and 126.0 V/s for resistances R_{mf} of 10 MΩ,100 MΩ,1 GΩ and 10 GΩ, respectively. The n–v and R_{mf}–v relationships resembled the relationships between n and dV/dt_{max} and R_{mf} and dV/dt_{max}, respectively.

Electrical Bridging via Fibroblast Inserts

Electrical bridging between two chains of myocytes coupled via a single fibroblast is demonstrated in Fig. 12. The resistance between myocytes R_{mm} was set to 6 MΩ. A myocyte–fibroblast resistance of R_{mf} of 10 MΩ caused a conduction delay Δ_t of 2.05 ms (Fig. 12a). A resistance R_{mf} of 17.416545 MΩ led to the maximal delay Δ_t of 18.2 ms (Fig. 12b). Conduction was blocked for resistances $R_{mf} \geq 17.416546$ MΩ (Fig. 12c).

The effect of the myocyte–myocyte resistance R_{mm} and myocyte–fibroblast resistance R_{mf} on conduction delays Δ_t caused by a single fibroblast is further explored in (Fig. 13). The myocyte–myocyte resistor R_{mm} was varied from 1 MΩ to 100 MΩ. For R_{mm} larger than 50 MΩ, conduction was blocked independent of the choice of R_{mf}. For each R_{mm} otherwise, Δ_t was an exponential-like monotonical increasing function of R_{mf} (Fig. 14). The maximal Δ_t amounted to 20.3 ms with a $R_{mm} = 50$ MΩ and $R_{mf} = 48.876354$ MΩ. Block of conduction occurred always for resistances R_{mf} larger than the one causing maximal Δ_t.

In order to explore the role of fibroblast's transmembrane currents in the development of conduction delays, a similar simulation as presented above was performed with an ohmic coupling of the myocyte chains (Fig. 15). A resistance between these chains R_{cc} of 20 MΩ led to a delay Δ_t between the two central myocytes of 2 ms (Fig. 15a). A resistance R_{cc} of 34.908765 MΩ caused the maximal conduction delay of 17.3 ms (Fig. 15b). Conduction was blocked for resistances $R_{cc} \geq 34.908766$ MΩ (Fig. 15c).

The effect of the myocyte–myocyte resistance R_{mm} and chain–chain resistance R_{cc} on conduction delays is demonstrated in Fig. 16. Similar as in simulations with the arrangement M_{21}–F_1–M_{21}, Δ_t was an exponential-like monotonical increasing function of R_{cc} for each R_{mm} and conduction block occurred for resistances R_{mf} larger than the one causing maximal Δ_t.

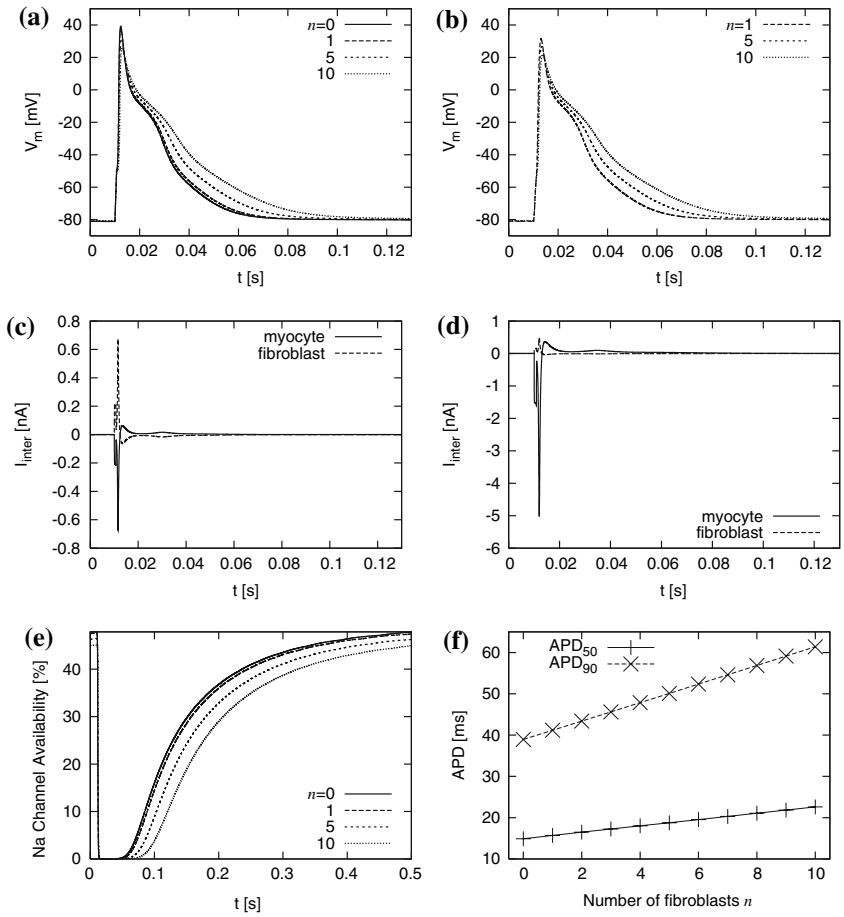

FIGURE 7. Myocyte–fibroblast interactions simulated with arrangement M–F$_n$ for an intercellular resistance R_{mf} of 100 MΩ. The transmembrane voltage V_m of (a) a myocyte and (b) fibroblasts were calculated for a number of fibroblasts n varying between 0 and 10. Intercellular currents I_{inter} in case of (c) a single and (d) 10 coupled fibroblasts flows during stimulus and upstroke from the myocyte to the fibroblast(s) followed by reflow at time of the action potential notch and repolarization. (e) Sodium channel availability was determined as product of the fast and slow inactivation gates. (f) The n-APD$_{50}$ and n-APD$_{90}$ relationships are positive.

Conduction delays Δ_t caused by insets of 3 and 5 fibroblasts are presented in Fig. 17. Again, the delay Δ_t was an exponential-like function of R_{mf} for each R_{mm}. Increasing numbers of inserted fibroblasts led to decreasing resistances R_{mf} leading to maximal Δ_t.

CONCLUSIONS AND DISCUSSION

Studies of electrical interactions between myocytes and fibroblasts are commonly carried out in cell cultures, which provide a controlled extracellular environment and allow versatile cell arrangement through appropriate seeding techniques. In this paper, we chose a computational approach to gain insights in the electrophysiology of coupled myocytes and fibroblasts with particular focus on bridging of conduction between myocytes via fibroblasts.

A mathematical fibroblast model was developed based on recent voltage clamp, pharmacological and PCR studies. This model is capable of reconstructing experimental ion channel activation kinetics and steady-state transmembrane currents for different voltages (Figs. 2 and 5). We used a Nernst and Goldman–Hodgkin–Katz equation based description for the major currents I_{Kir} and I_{Shkr}, respectively, to allow reconstruction of measurement data for a wide range of $[K^+]_o$ (5–100 mM). The resting transmembrane voltage was set to −58 mV for $[K^+]_o$ = 5 mM according to measurement data.[43] Other studies indicated a wide range of resting voltages.[23,24] The described fibroblast model might provide a framework for the description of myofibroblasts, which have been considered to have the same major ionic currents.[8]

In addition to the fibroblast model, we used the Pandit *et al.* rat ventricular myocyte model[34] and an electrical conduction model to characterize myocyte–fibroblasts interactions. Results from our simulations, in which a single myocyte was coupled to a number of

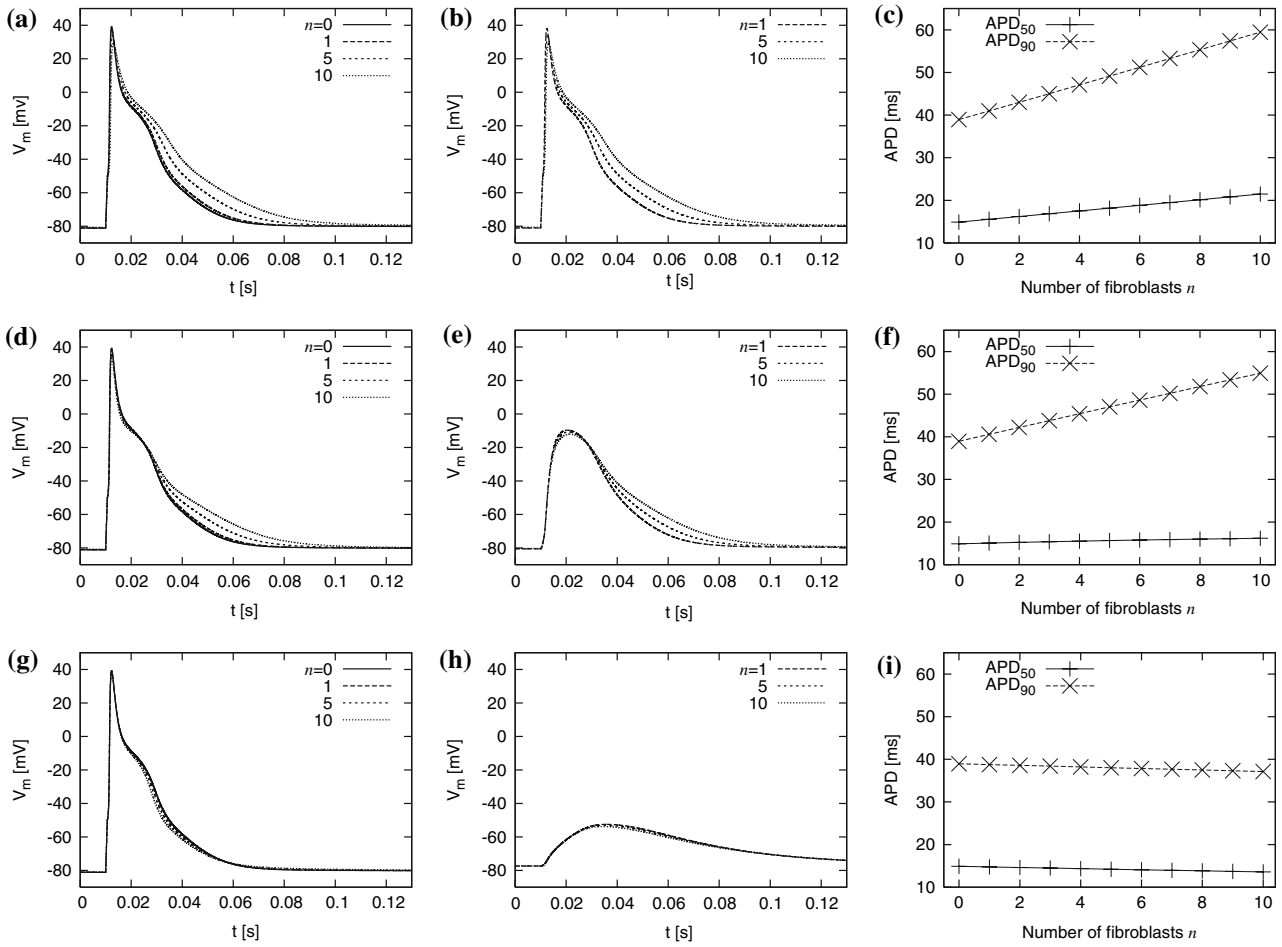

FIGURE 8. Myocyte–fibroblast interactions simulated with arrangement M–F$_n$. The number of fibroblasts n was varied between 0 and 10. A resistance R_{mf} of (a–c) 10 MΩ, (d–f) 1 GΩ, and (g–h) 10 GΩ was chosen. The transmembrane voltage V_m of (a, d, g) a myocyte and (b, e, h) fibroblasts as well as (c, f, i) the APDs of the myocyte are shown for various resistances and numbers of coupled fibroblasts.

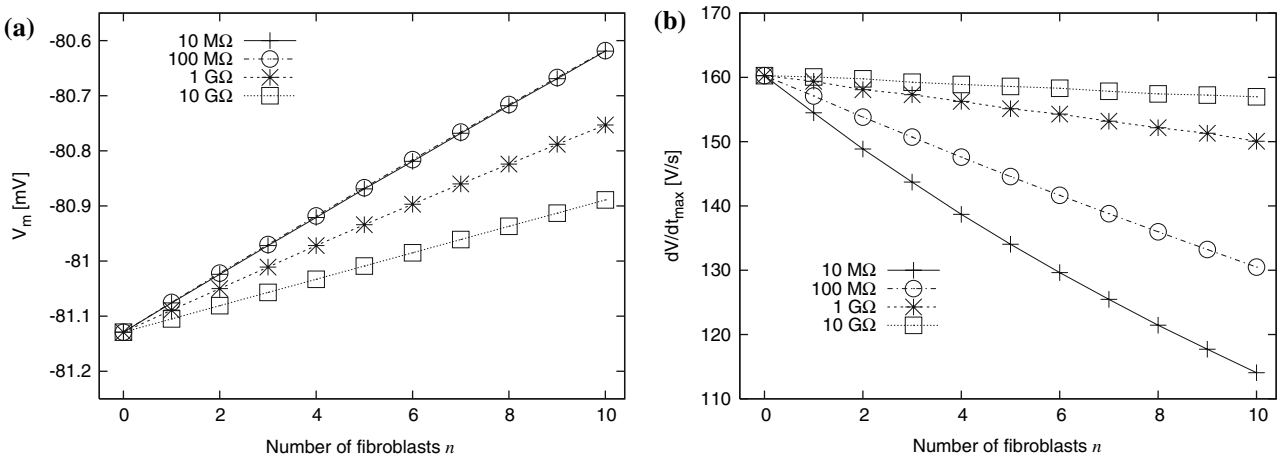

FIGURE 9. Electrophysiological quantification in arrangement M–F$_n$. (a) Resting transmembrane voltage and (b) maximal upstroke velocity were determined for the myocyte. Fibroblasts increase marginally the resting voltage, but modulate significantly upstroke velocity.

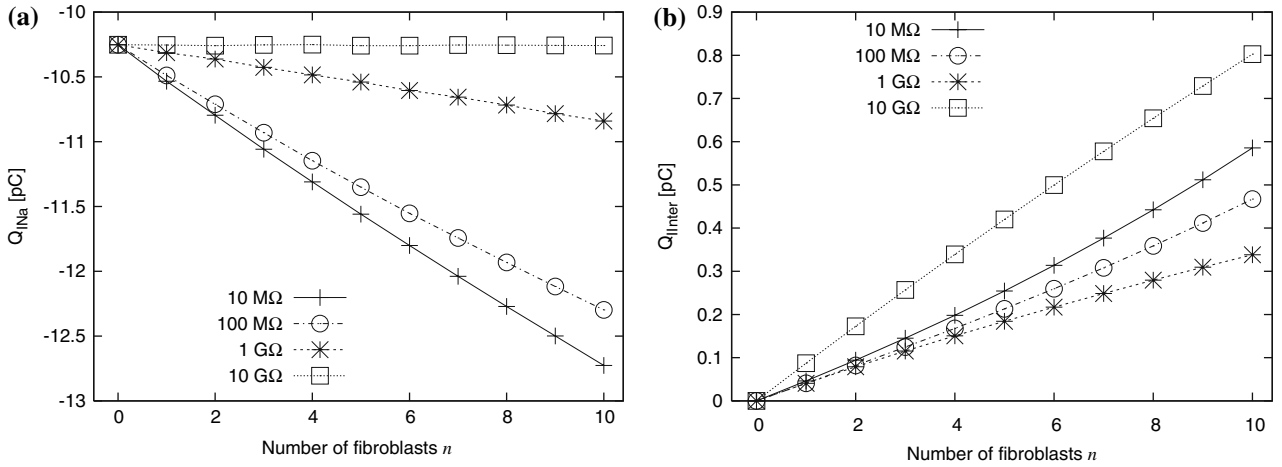

FIGURE 10. Charge movement in arrangement M–F$_n$. (a) Charge passing through sodium channels Q_{INa} and (b) charge associated with intercellular current Q_{IInter} were determined for the myocyte. Negative values indicate summary transport of positive charge into the myocyte. High and average coupled fibroblasts increase the magnitude of Q_{INa} and act as sink for intercellular current.

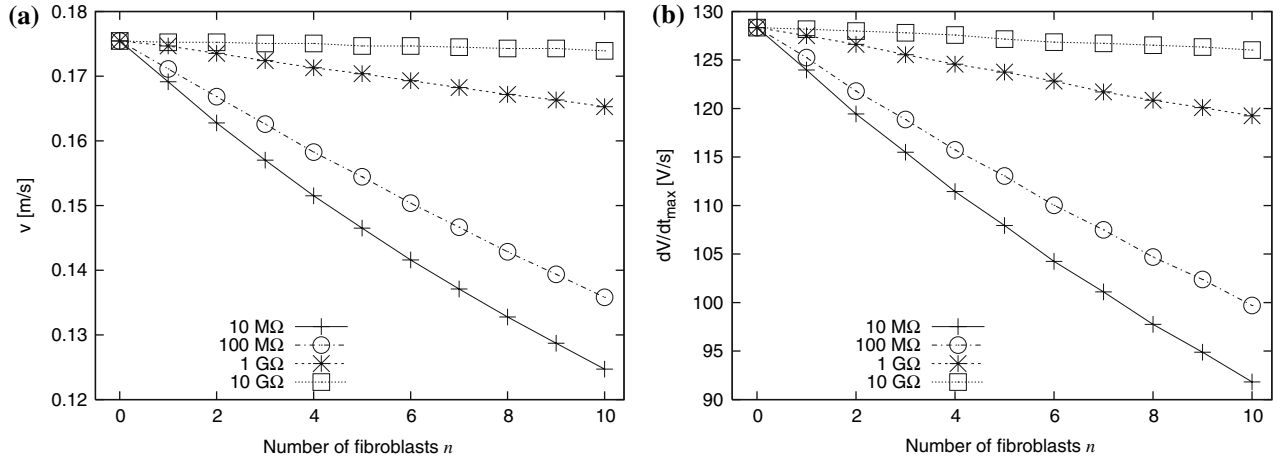

FIGURE 11. (a) Conduction velocity in myocyte chain and (b) upstroke velocity simulated with arrangement M$_{32}$–F$_{nx32}$. The resistance between myocytes R_{mm} was set to 6 MΩ. The resistance between myocytes and fibroblasts was varied between 10 MΩ and 10 GΩ. Coupling to fibroblasts reduced conduction velocity and upstroke velocity in a strand of myocytes.

fibroblasts (M–F$_n$), indicate that coupled fibroblasts can have a significant effect on the dynamics of myocyte depolarization (Figs. 7f and 8c, f). However, in all simulations myocytes developed an action potential with peak voltage above 30 mV. In ventricular myocytes the depolarization is commonly initiated by inflow of intercellular or stimulus current causing large sodium currents. We found that the charge associated with sodium inflow Q_{INa} was an approximately linear function of the number of coupled fibroblasts (Fig. 10a). This additional inflow is mostly used to charge the fibroblast membrane and raise their resting voltages (Figs. 7b and 8b, e, h). Thus, myocytes were able to compensate for the additional electrical load of coupled fibroblasts by increasing sodium channel current I_{Na}. Simulations with two models of guinea pig ventricular myocytes[30,38] showed similar relationships (data not shown).

A re-flow of this additional charge from fibroblasts to the myocyte occurred during repolarization for average and high coupling (Fig. 7c, d). This re-flow reduced repolarization and caused increased APDs (Figs. 7f and 8c, f). In case of marginal coupling, charging of fibroblast membranes was decelerated and still ongoing during early repolarization. The re-flow started in the terminal phase of repolarization.

The charge transported through gap junctions Q_{IInter} from the myocyte to high and average coupled fibroblasts was positive during an action potential (Fig. 10b). Thus, these fibroblasts act as an electrical

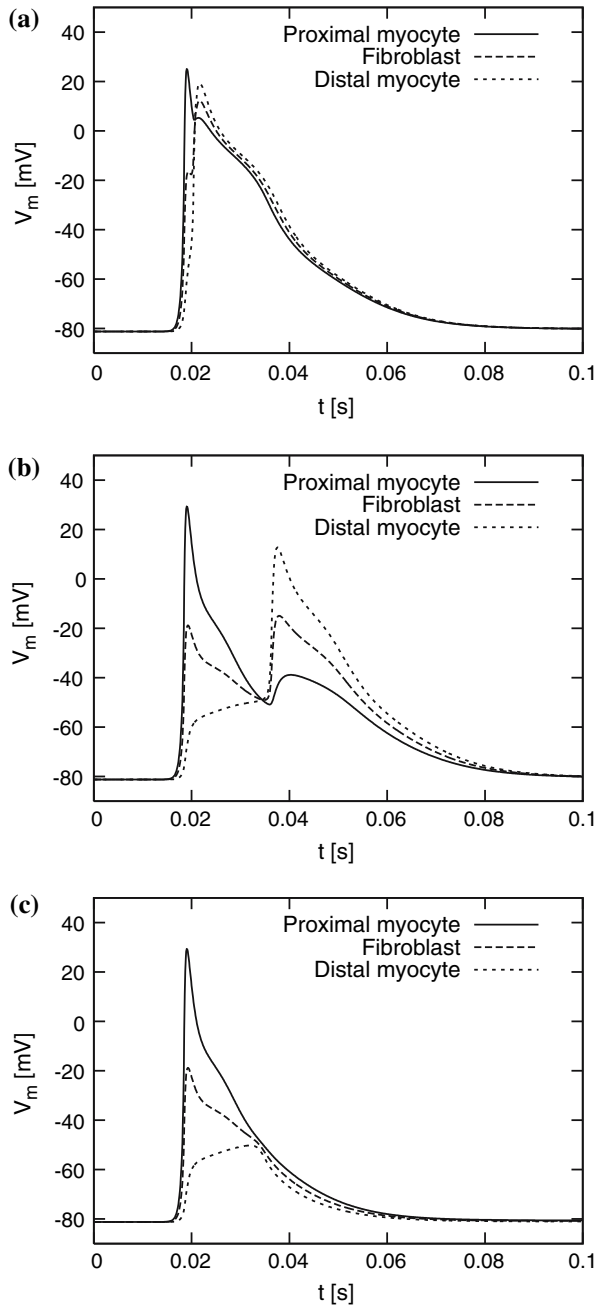

FIGURE 12. Myocyte–fibroblast interactions simulated with arrangement M_{21}–F_1–M_{21}. The transmembrane voltage V_m of the central fibroblast as well as its proximal and distal myocyte is shown. A myocyte–myocyte resistor $R_{mm} = 6\,M\Omega$ and myocyte–fibroblast resistor R_{mf} of (a) 10 MΩ, (b) 17.416545 MΩ and (c) 17.416546 MΩ was chosen, which led to conduction, delayed conduction and block, respectively.

sink. However, the magnitude of Q_{IInter} was less than 25% of the increase of the magnitude of Q_{INa} caused by coupled fibroblasts (Fig. 10a vs. 10b). Thus, more than 75% of the additional Q_{IInter} was associated to the myocyte and applied at least partly for decelerated repolarization. A similarly decelerated repolarization was not found in our simulations with models of guinea pig ventricular myocytes (data not shown).

Our simulations of a strand of myocytes indicate that increased coupling of fibroblasts can significantly reduce conduction velocity in cardiac tissue (Fig. 11a). We suggest that this effect is caused by reduction of myocyte upstroke velocity (Fig. 11b), which was similarly visible in our studies of a single myocyte coupled to a number of fibroblasts (Fig. 9b). Decreased upstroke velocity in the strand studies compared to those in the single myocyte studies can be explained by intercellular electrical coupling. Repolarized neighboring myocytes act as electrical sinks for an excited cell. Intercellular current flow from a cell undergoing upstroke into depolarized myocytes reduces upstroke velocity.

Conduction velocity determined in our myocyte strand simulations is small in comparison to velocities from experimental studies with cardiac tissue of rat[44] and other mammals.[13,35] Those studies were carried out at physiological temperature. Experimental studies of cardiac tissue reported a reduced conduction velocity at room temperature quantitatively similar as in our simulations.[41]

Conduction block did not occur in the myocyte strand simulations with 0–10 coupled fibroblasts. However, we expect that for a larger number of coupled fibroblasts the conduction velocity would further decrease and block might occur. We suggest that an analysis applying the safety factor concept[42] would give detailed insights in block conditions.

Evidence for bridging of electrical conduction in cardiac tissue via fibroblast insets was provided by experimental studies of cell culture[14] and computational studies with a one-dimensional cardiac fiber model.[46] These studies showed reduced conduction velocity and upstroke velocity in fibroblast insets. Length of the insets was positively correlated with the conduction delay Δ_t. Large variances of Δ_t were presented in the experimental study with insets consisting of fibroblasts and also HeLa cells expressing Cx43 gap junctions.

Our studies of electrical bridging reconstructed the experimentally found increase of Δ_t with inset length. The studies were carried out in a one-dimensional model consisting of two chains of myocytes connected by a chain of fibroblasts. Increased Δ_t for increased number of inserted fibroblasts are demonstrated in Figs. 17b, d and 13b for a wide range of R_{mm} and R_{mf}. Maximal conduction delays in our studies were smaller than in the experimental study, which might be attributed to electrophysiological differences of neonatal cells used in the cell culture studies and our models describing adult cells. In our studies, conduction block occurred at significantly smaller than

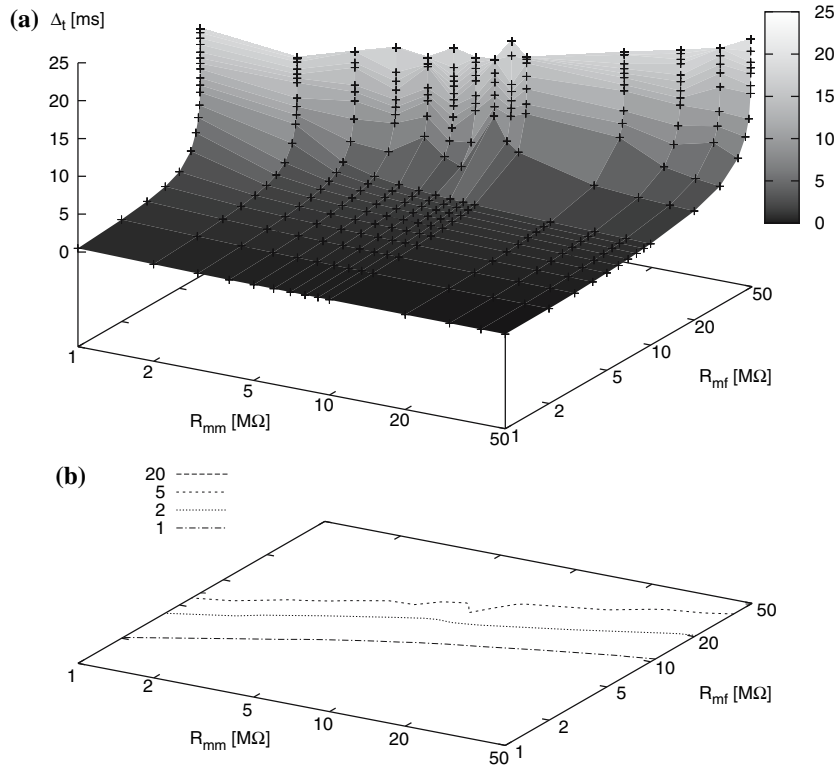

FIGURE 13. Conduction delays Δ_t simulated with arrangement M_{21}–F_1–M_{21}. Myocyte–myocyte resistances R_{mm} and myocyte–fibroblast resistances R_{mf} were varied. The resulting conduction delays were visualized (a) as three-dimensional plot and (b) with isolines. Each simulated conduction delays is marked with a cross (+).

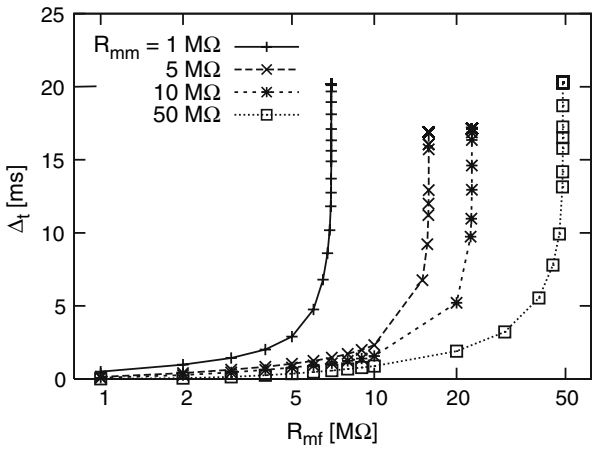

FIGURE 14. Exemplary conduction delays Δ_t simulated with arrangement M_{21}–F_1–M_{21}. Delays for myocyte–myocyte resistances R_{mm} of 1, 5, 10, and 50 MΩ are shown.

reported values of resistors of myocyte–fibroblast and fibroblast–fibroblast pairs. A possible explanation for this underestimation is parallel connection of fibroblasts in the inset. We expect that using 2- and 3-dimensional continuum modeling approaches will improve the reconstruction of the cell culture studies. Furthermore, these modeling approaches would simplify the reconstruction of experiments with myocyte–fibroblast mixtures in insets and anisotropy of intercellular coupling.

A major goal of our bridging studies was the characterization of Δ_t in relationship to coupling resistances and number of fibroblasts. We found an exponential relationship between the myocyte–fibroblast resistance R_{mf} and Δ_t. The value of R_{mf} for maximal Δ_t and for conduction block differed by only 1 Ω, which presented the resolution limit for the maxima detection.

An exponential relationship was also found in our studies of ohmic coupled two myocyte chains with respect to the chain–chain resistor R_{cc} and Δ_t (Fig. 16). Results of these simulations were very close to the results with a single fibroblast inset when R_{mf} was twice of R_{ss}. These studies revealed that ion channel and capacitive currents of fibroblasts play a minor role for the spread of the excitation at least with small numbers of fibroblasts in the inset.

Limitations of the Presented Studies

We did not adopt, develop, or apply descriptions of mechano-electrical feedback in fibroblasts and myocytes. Mechanosensitive currents of fibroblasts have

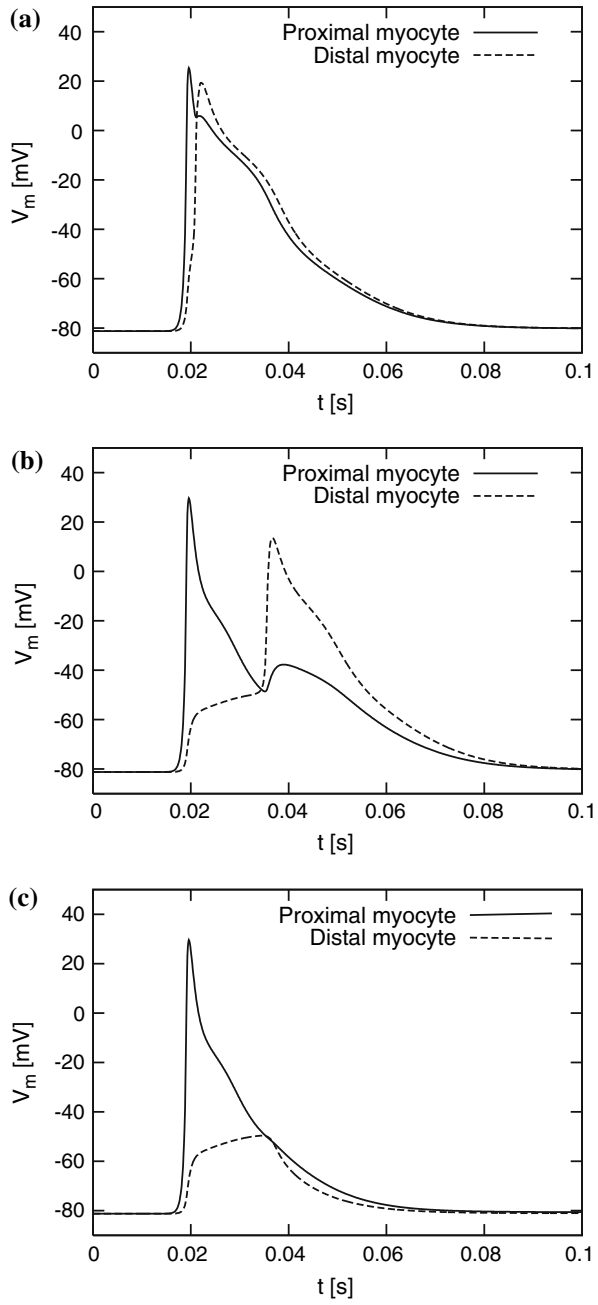

FIGURE 15. Bridging simulated with arrangement M_{21}–M_{21}. The myocyte–myocyte resistors R_{mm} inside of each chain were fixed to 6 MΩ. The chains were coupled with a resistor of R_{cc} of (a) 20 MΩ, (b) 34.908765 MΩ and (c) 34.908766 MΩ, which led to conduction, delayed conduction and block, respectively. The transmembrane voltage V_m of two myocytes proximal and distal to the varied resistor R_{cc} is shown.

been described in the sino-atrial node and atrium.[22,23,27] Mechano-electrical feedback is affecting the transmembrane voltage and ion concentrations of cardiac myocytes particularly for high strain and cell swelling.[32,39,40] Most of these feedback mechanisms are still subject of controversies with respect to their modulation and effects on cardiac tissue *in vivo*. Commonly, these effects are ignored in computational studies of cardiac electrophysiology.

Another limitation of this paper results from the weak experimental characterization of currents other than I_{Kir} and I_{Shkr} in myocardial fibroblasts. Our definition of I_b was adapted from models of kidney and cardiac fibroblasts.[28,45] The choice of its reversal potential E_b is based on experimental studies of rat kidney fibroblasts[18] and reflects our assumption that the current has several contributors. We expect that future models will decompose I_b in several currents and comprise intracellular ion handing in more detail as experimental evidence and quantitative data becomes available. Particular candidates are the ubiquitous sodium–potassium pump, L-type calcium and calcium-activated chloride currents. The latter two candidates are prominent in rat kidney fibroblasts.[18]

Our description of fibroblasts neglects steady-state inactivation of K^+ currents, which was reported by Shibukawa and colleagues.[43] The inactivation was characterized by stepping to a membrane voltage of 50 mV from holding voltages V_h in the range of −90 to +10 mV applied for 30 s. This steady-state inactivation was negligible for voltages $V_h \leq -70$ mV and not visible in the clamping protocol with 400 ms voltage steps from a holding potential of −90 mV (Fig. 5a, b). Thus, only marginal effects of steady-state inactivation can be expected with the protocols described in our work.

Our simulations did not produce evidence for reflected reentry via fibroblast insets. However, only a small subset of parameters was varied in these studies. Thus, in general we cannot reject reflected reentry as an electrophysiological phenomenon related to myocyte–fibroblast interactions. We suggest that in our studies the absence can be explained by electrophysiological properties of the sodium channels. Sodium channel availability is ruled by fast and slow inactivation processes (Fig. 7e). In our simulations the availability of sodium channels in the proximal myocyte was marginal during upstroke of the distal myocyte. Reactivation of sodium currents in the proximal myocyte was prohibited despite significant depolarization by currents from the distal myocyte via the fibroblast insert (Fig. 12b). Also the computational studies of Vasquez and colleagues did not show evidence for reflected reentry despite long conduction delays up to 50.4 ms [1000]. These studies were performed with a model of guinea pig ventricular myocytes [1000], which have a long action potential duration relative to rat ventricular myocytes. Also in these studies, sodium channel inactivation explains the absence of reentry.

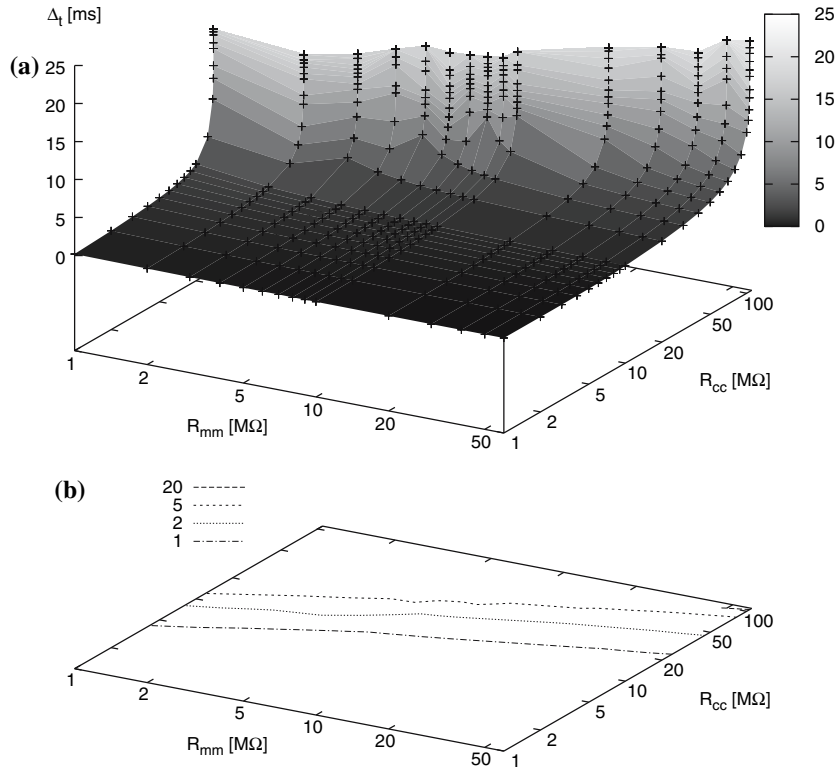

FIGURE 16. Conduction delays Δ_t simulated with arrangement M_{21}–M_{21} visualized (a) as three-dimensional plot and (b) with isolines. Myocyte–myocyte resistances R_{mm} and chain–chain resistance R_{cc} were varied.

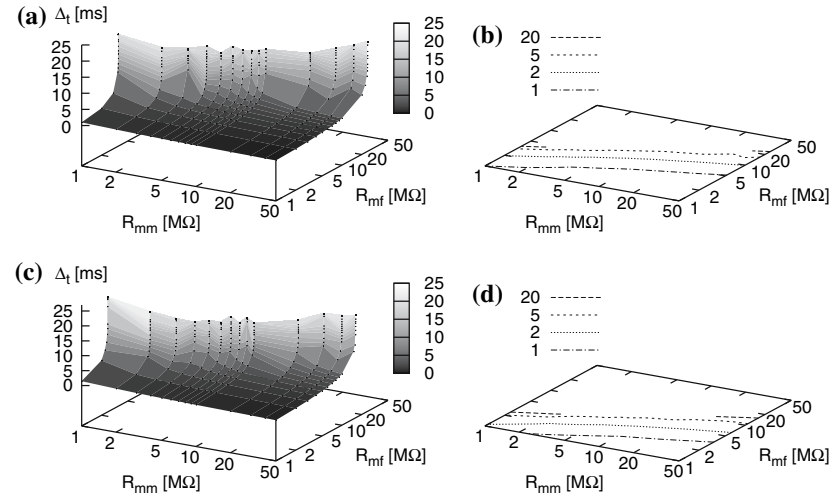

FIGURE 17. Conduction delays Δ_t simulated with arrangement (a, b) M_{21}–F_3–M_{21} and (c, d) M_{21}–F_5–M_{21}. Myocyte–myocyte resistances R_{mm} and myocyte–fibroblast resistances R_{mf} were varied. The resulting conduction delays were visualized (a, c) as three-dimensional plot and (b, d) with isolines.

In our simulations, we applied models which describe mean electrophysiological properties of cardiac cells according to recently published experimental data.[43] As in most computational studies, variabilities of properties were not taken into account, despite these are partly very significant and might severely affect simulation results. Particularly, resting voltage and membrane capacity show a large variability in cardiac fibroblasts.[23,24,37] We expect that novel stochastic approaches will allow to take these variabilities into consideration and thus increase the significance of this and similar computational studies.[15]

ACKNOWLEDGMENTS

This work has been supported by the Richard A. and Nora Eccles Fund for Cardiovascular Research, awards from the Nora Eccles Treadwell Foundation (FBS, APM, JAA), and NIH/NHLBI, HL63969 (APM). We thank Ms. Catherine Lloyd, University of Auckland, and Dr. Alan Garny, University of Oxford, for implementing a CellML version of the fibroblast model. We acknowledge the support of Prof. James B. Bassingthwaighte and Dr. Brian Carlson, University of Washington, for implementation of the fibroblast and myocyte-fibroblast models in JSim and including these in the model repository of the NSR Physiome Project (http://www.physiome.org/model/doku.php?id=Cell_Physiology:Fibroblast:model_index and http://www.physiome.org/model/doku.php?id=Cell_Physiology:Action_potential:Myocyte_fibroblast_coupling:model_index).

REFERENCES

[1]Antzelevitch, C., and A. Lukas. Reflection and circus movement reentry in isolated atrial and ventricular tissue. In: Electrophysiology and Pharmacology of the Heart, edited by K. H. Dangman and D. S. Miura. Marcel Dekker, 1991, Chapter 11, pp. 251–275.

[2]Brown, R. D., S. K. Ambler, M. D. Mitchell, and C. S. Long. The cardiac fibroblast: therapeutic target in myocardial remodeling and failure. *Annu. Rev. Pharmacol. Toxicol.* 45:657–687, 2005.

[3]Cabo, C., and R. C. Barr. Reflection after delayed excitation in a computer model of a single fiber. *Circ. Res.* 71:260–270, 1992.

[4]Camelliti, P., G. P. Devlin, K. G. Matthews, P. Kohl, and C. R. Green. Spatially and temporally distinct expression of connexins after sheep ventricular infarction. *Cardiovas. Res.* 62:415–425, 2004.

[5]Camelliti, P., C. R. Green, I. LeGrice, and P. Kohl. Fibroblast network in rabbit sinoatrial node: structural and functional identification of homogeneous and heterogeneous cell coupling. *Circ. Res.* 94(6):828–835, 2004.

[6]Camelliti, P., and P. Kohl. Myocyte/fibroblast 2D structured cardiac tissue model. *J. Phyiol.* 552P:P36, 2003.

[7]Camelliti, P., A. D. McCulloch, and P. Kohl. Microstructured cocultures of cardiac myocytes and fibroblasts: a two-dimensional in vitro model of cardiac tissue. *Microsc. Microanal.* 11:249–259, 2005.

[8]Chilton, L., S. Ohya, D. Freed, E. George, V. Drobic, Y. Shibukawa, K. A. MacCannel, Y. Imaizumi, R. B. Clark, M. C. Dixon, and W. R. Giles. K^+ currents regulate the resting membrane potential, proliferation, and contractile response in ventricular fibroblasts and myofibroblasts. *Am. J. Physiol. Heart Circ. Physiol.* 288:H2931–H2939, 2005.

[9]Cranefield, P. F., and B. F. Hoffmann. Conduction of the cardiac impulse: II. summation and inhibition. *Circ. Res.* 28:220–233, 1971.

[10]Cranefield, P. F., H. O. Klein, and B. F. Hoffmann. Conduction of the cardiac impulse: I. Delay, block, and one-way block in depressed Purkinje fibers. *Circulation* 28:199–219, 1971.

[11]Cranefield, P. F., A. L. Wit, and B. F. Hoffmann. Conduction of the cardiac impulse: III. Characteristics of slow conduction. *Circ. Res.* 59:227–246, 1971.

[12]Eghbali, M., M. J. Czaja, M. Zeydel, F. R. Weiner, M. A. Zern, S. Seifter, and O. O. Blumenfeld. Collagen chain mRNAs in isolated heart cells from young and adult rats. *J. Mol. Cell. Cardiol.* 20:267–276, 1988.

[13]Fleischhauer, J., L. Lehmann, and A. G. Kĺeber. Electrical resistances of interstitial and microvascular space a determinants of the extracellular electrical field and velocity of propagation in ventricular myocardium. *Circulation* 92:587–594, 1995.

[14]Gaudesius, G., M. Miragoli, S. P. Thomas, and S. Rohr. Coupling of cardiac electrical activity over extended distances by fibroblasts of cardiac origin. *Circ. Res.* 93:421–428, 2003.

[15]Geneser, S. E., R. M. Kirby, and F. B. Sachse. Sensitivity analysis of cardiac electrophysiological models using polynomial chaos. *Proc. IEEE EMBS* 4:4042–4045, 2005.

[16]Goldsmith, E. C., A. Hoffman, M. O. Morales, J. D. Potts, R. L. Price, A. McFadden, M. Rice, and T. K. Borg. Organization of fibroblasts in the heart. *Dev. Dynam.* 230:787–794, 2004.

[17]Goshima, K. Synchronized beating of and electrotonic transmission between myocardial cells mediated by heterotypic strain cells in a monolayer culture. *Exp. Cell Res.* 58:420–426, 1969.

[18]Harks, E. G., J. J. Torres, L. N. Cornelisse, D. L. Ypey, and A. P. Theuvenet. Ionic basis for excitability of normal rat kidney (NRK) fibroblasts. *J. Cell Physiol.* 196(3):493–503, 2003.

[19]B. Hille. *Ionic Channels of Excitable Membranes*, 2nd edition. Sinauer Associates, 1992.

[20]Hyde, A., B. Blondel, A. Matter, J. P. Cheneval, B. Filloux, and L. Girardier. Homo- and heterocellular junctions in cell cultures: an electrophysiological and morphological study. *Prog. Brain Res.* 31:283–311, 1969.

[21]Iyer, V., R. Mazhari, and R. L. Winslow. A computational model of the human left-ventricular epicardial myocyte. *Biophys. J.* 87(3):1507–1525, 2004.

[22]Kamkin, A., I. Kiseleva, I. Lozinsky, and H. Scholz. Electrical interaction of mechanosensitive fibroblasts and myocytes in the heart. *Basic Res. Cardiol.* 100:337–345, 2005.

[23]Kamkin, A., I. Kiseleva, K.-D. Wagner, A. Pylaev, K. P. Leiterer, H. Theres, H. Scholz, J. Günther, and G. Isenberg. A possible role for atrial fibroblasts in postinfarction bradycardia. *Am. J. Physiol.* 282:H842–H849, 2002.

[24]Kiseleva, I., A. Kamkin, A. Pylaev, D. Kondratjev, K. P. Leiterer, H. Theres, K. D. Wagner, P. B. Persson, and J. Gunther. Electrophysiological properties of mechanosensitive atrial fibroblasts from chronic infarcted rat heart. *J. Mol. Cell. Cardiol.* 30(6):1083–1093, 1998.

[25]Klemic, K. G., D. M. Durand, and S. W. Jones. Activation kinetics of the delayed rectifier potassium current of bullfrog sympathetic neurons. *J. Neurophysiol.* 79:2345–2357, 1998.

[26]Kohl, P., P. Camelliti, F. L. Burton, and G. L. Smith. Electrical coupling of fibroblasts and myocytes: relevance for cardiac propagation. *J. Electrocardiol.* 38:45–50, 2005.

[27]Kohl, P., A. G. Kamkin, I. S. Kiseleva, and D. Noble. Mechanosensitive fibroblasts in the sino-atrial node region of the rat heart: interaction with cardiomyocytes and possible role. *Exp. Physiol.* 79:943–956, 1994.

[28]Kohl, P., and D. Noble. Mechanosensitive connective tissue: potential influence on heart rhythm. *Cardiovasc. Res.* 32:62–68, 1996.
[29]Luo, C.-H., and Y. Rudy. A dynamic model of the ventricular cardiac action potential: I. Simulations of ionic currents and concentration changes. *Circ. Res.* 74(6):1071–1096, 1994.
[30]Luo, C.-H., and Y. Rudy. A dynamic model of the ventricular cardiac action potential: II. Afterdepolarizations, triggered activity, and potentiation. *Circ. Res.* 74(6):1097–1113, 1994.
[31]Manabe, I., T. Shindo, and R. Nagai. Gene expression in fibroblasts and fibrosis: involvement in cardiac hypertrophy. *Circ. Res.* 91:1103–1113, 2005.
[32]Nishimura, S., Y. Kawai, T. Nakajima, Y. Hosoya, H. Fujita, M. Katoh, H. Yamashita, R. Nagai, and S. Sugiura. Membrane potential of rat ventricular myocytes responds to axial stretch in phase, amplitude and speed-dependent manners. *Cardiovasc. Res.* 72:403–411, 2006.
[33]Noble, D., A. Varghese, P. Kohl, and P. Noble. Improved guinea-pig ventricular cell model incorporating a diadic space, I_{Kr} and I_{Ks}, and length- and tension-dependent processes. *Can. J. Cardiol.* 14(1):123–134, 1998.
[34]Pandit, S. V., R. B. Clark, W. R. Giles, and S. S. Demir. A mathematical model of action potential heterogeneity in adult left ventricular myocytes. *Biophys. J.* 81:3029–3051, 2001.
[35]Penefsky, Z. J., and B. F. Hoffman. Effects of stretch on mechanical and electrical properties of cardiac muscle. *Am. J. Physiol.* 204(3):433–438, 1963.
[36]Press, W. H., S. A. Teukolsky, W. T. Vetterling, and B. P. Flannery. Numerical Recipes in C. 2nd ed., Cambridge, New York, Melbourne: Cambridge University Press, 1992.
[37]Rook, M. B., A. C. G. van Ginneken, B. de Jonge, A. El Aoumari, D. Gros, and H. J. Jongsma. Differences in gap junction channels between cardiac myocytes, fibroblasts, and heterologous pairs. *Am. J. Physiol.* 263:C959–C977, 1992.
[38]Rudy, Y. Conductive bridges in cardiac tissue: a beneficial role or an arrhythmogenic substrate. *Circ. Res.* 94:709–711, 2004.
[39]Ruknudin, A., F. Sachs, and J. O. Bustamante. Stretch-activated ion channels in tissue-cultured chick heart. *Am. J. Physiol. Heart Circ. Physiol* 264(33):H960–972, 1993.
[40]Sachse, F. B. Computational Cardiology: Modeling of Anatomy, Electrophysiology, and Mechanics. LNCS 2966. Heidelberg:Springer Press, 2004.
[41]Sano, T., N. Takayama, and T. Shimamoto. Directional difference of conduction velocity in the cardiac ventricular syncytium studied by microelectrodes. *Circ. Res.* 7:262–267, 1959.
[42]Shaw, R. M., and Y. Rudy. Ionic mechanisms of propagation in cardiac tissue: roles of the sodium and L-type calcium currents during reduced excitability and decreased gap junction coupling. *Circ. Res.* 81:727–741, 1997.
[43]Shibukawa, Y., L. Chilton, K. A. MacCannell, R. B. Clark, and W. R. Giles. K^+ currents activated by depolarization in cardiac fibroblasts. *Biophys. J.* 88:3924–3935, 2005.
[44]Spear, J. F., and E. N. Moore. Stretch-induced excitation and conduction disturbances in the isolated rat myocardium. *J. Electrocardiol.* 5(1):15–24, 1972.
[45]Torres, J. J., L. N. Cornelisse, E. G. A. Harks, W. P. M. van Meerwijk, A. P. R. Theuvenet, and D. L. Ypey. Modeling action potential generation and propagation in NRK fibroblasts. *Am. J. Physiol.* 287:H851–H865, 2004.
[46]Vasquez, C., A. P. Moreno, and E. J. Berbari. Modeling fibroblast–mediated conduction in the ventricle. *Proc. CiC* 31:349–352, 2004.
[47]Wit, A. L., P. F. Cranefield, and B. F. Hoffman. Slow conduction and reentry in the ventricular conduction system: II. Single and sustained circus movement in networks of canine and bovine Purkinje fibers. *Circ. Res.* 30:11–22, 1972.
[48]Wit, A. L., B. F. Hoffman, and P. F. Cranefield. Slow conduction and reentry in the ventricular conduction system: I. Return extrasystole in the canine Purkinje fibers. *Circ. Res.* 30(1):1–10, 1972.
[49]Zagotta, W. N., and R. W. Aldrich. Voltage-dependent gating of Shaker A-type potassium channels in drosophila muscle. *J. Gen. Physiol.* 95(1):29–60, 1990.